

Two-step forming for improvement of forming limit in rotary nosing with relieved die for fabrication of axisymmetric and eccentric nosed tubes

Wataru Oba^a, Yusuke Imaizumi^a, Shohei Kajikawa^a, Takashi Kuboki^{a*}

^aDepartment of Mechanical and Intelligent Systems Engineering, University of Electro-Communications, 1-5-1 Chofu Gaoka, Chofu Tokyo, 182-8585, Japan

*Corresponding author. Tel.: +81-042-443-5410,

E-mail: kuboki@mce.uec.ac.jp

ABSTRACT

This paper presents application of two-step forming for improving the forming limit in rotary nosing with a relieved die. Nosing is one method which is used for reducing the diameter of a tube tip. "Two-step nosing" is composed of two stages and different dies are applied for the two stages. The die shapes are determined based on the occurrence tendency of defects in "one-step nosing", where only one die is used through the whole process. In this research, a series of experiments and numerical analyses of one-step nosing was carried out for investigating the mechanism of the occurrence of defects. As a result, it is revealed that the occurrence of defects was highly relevant with the contact area between the die and tube. Based on the result of one-step nosing, the optimum die shapes were determined for the two stages, and then "two-step nosing" improved the forming limit 9 % higher than one-step nosing under the optimum condition. Furthermore, "two-step nosing" was experimentally applied for forming eccentric nosed tubes, and its superiority was verified.

Keywords: nosing, aluminum, tool geometry, spinning

1. Introduction

Nosing is a reduction method of tube tips by applying circumferential compressive stress using rigid tools. Nosing is used for fabrication of various products, including structural tubes in buildings or machines, mufflers of motorcycles and vehicles, resealable cans with bottle shape and so on. Press forming and spinning are well known examples of nosing processes. In press forming, a tube is pressed into an axisymmetric cone die and the tube tip is deformed. Manabe and Nishimura (1984) summarized the mechanism of the nosing process based on experimental and theoretical investigation. Alves et al. (2006) investigated the expansion and reduction of a tube tip in order to clarify the effect of process parameters on the forming limit induced by some defects. Although the working process of press forming is simple and the productivity is high, the forming limit is low due to occurrence of some defects by the large working force. In spinning, on the other hand, a tool of a roller or bar contacts with a rotating tube and the tube is deformed by the tool, which moves back and forth on the worked surface. Kobayashi and Yoshimura (2011) proposed a method for generating an optimum tool path for the nosing process in spinning based on the Fuzzy Model, and Zoghi et al. (2012) investigated the effect of the contact area and spinning feed speed on the deformation behaviour of a tube in tube spinning. C. Becker et al. (2014) described a process, which combines the continuous bending process with an incremental tube spinning process, which allows suppression of springback in the continuous bending process. Although the forming limit of spinning is higher than press forming, the productivity is much lower as the deformation is small per one path of tool movement. Thus, press forming is superior in productivity and spinning is superior in formability. However, a method with both superior formability and productivity had not been established.

Rotary nosing with a relieved die was proposed by the authors, and their previous research works revealed that the proposed method realizes both high formability and productivity without heat generation so as to maintain the material strength. Kuboki et al. (2008) reported the effect of forming condition on formability in rotary nosing with a relieved die. As a result, the previous work attained a high limit nosing ratio of 49 %, against 10 % in press forming, by optimizing the working condition for practically-used aluminum alloy A6063 with a thickness ratio of 1.7%. All the previous studies assumed that nosing should be conducted in a "one-step" manner. That is to say, nosing was conducted using only one relieved die through the whole process. However, usage of different relieved dies might be more effective, as multiple steps of forming are effective for attaining higher forming limits in other

metal forming methods, such as deep drawing. For example, Katoh et al. (1995) worked on research for the increase of cup height by the redrawing process.

This paper presents "two-step nosing" for improvement of the forming limit in rotary nosing with a relieved die. Two-step nosing applies two dies with different contact areas between the die and tube for the first and second stages in the nosing process. The optimum die shapes for the two steps are determined based on the results in one-step nosing. Therefore, in this research, a series of experiments and numerical analyses of one-step nosing were carried out as a preliminary investigation, and two-step nosing was thereafter carried out to clarify its validity.

Furthermore, additional experiments were carried out for investigation of the applicability of two-step nosing to fabrication of eccentric tubes, which have different axes for the nose tip and the base part of the tube. The eccentric tubes are expected to be used for catalyst cases, pipe-connecting parts and so on. In the experiments, the effect of eccentricity on formability was clarified and improvement of the forming limit was attempted by the application of two-step nosing. In addition, "slant nosing" was proposed for examining the moving path of a tube for forming eccentric tubes. In slant nosing, a tube is coaxially arranged to the die at the beginning of nosing, and incremental displacement in a direction perpendicular to the central axis of the die is applied to a tube while the tube is pushed into the die. The forming limit should be improved by suppression of partial deformation which is caused by partial contact of the tube tip to the die.

2. Rotary nosing with relieved die for reduction of tube tip

A schematic of rotary nosing with a relieved die is shown in Fig. 1. In this method, a tube is relatively pressed into a relieved die while rotating one of them. The relieved die is composed of contact and relieved surfaces. The relieved surfaces are designed not to contact the tube. Kuboki et al. (2015) reported the availability of the relieved die for improvement of the forming limit in forming a nosed tube. As the relieved surfaces have a function that weakens the axial pushing force that causes buckling and compressive hoop stress on the tube tip producing wrinkle, the forming limit is improved. The defect mode in rotary nosing with a relieved die is shown in Fig. 2. Four types of defects were observed and they were (a) split, (b) polygonal wrinkle, (c) buckling and (d) wrinkle. The occurrence tendency of those defects varied depending on the contact area between the die and tube. Therefore, it

would be significant to clarify the mechanism of defect occurrence and the effect of the contact area for improvement of the forming limit.

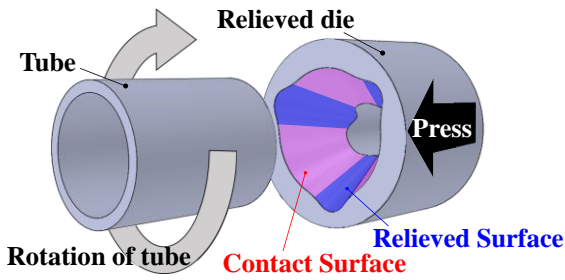


Fig. 1. Rotary nosing with relieved die for reduction of tube tip.

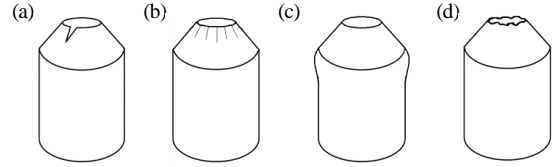


Fig. 2. Defect modes.

(a) Split, (b) Polygonal wrinkle, (c) Buckling, (d) Wrinkle.

3. One-step nosing

3.1. Forming conditions

A series of experiments and numerical analyses of one-step nosing were carried out in order to clarify the effect of the contact angle of the relieved die on the forming limit and defect occurrence. A photograph of the experimental set-up is shown in Fig. 3. A lathe was used for nosing. A die was clamped and rotated by the chuck of the lathe, and a tube was set on the tool stand and pushed into the die at a constant velocity. An outline of a relieved die and tube is shown in Fig. 4. When the contact angle γ is zero, the die and the tube contact on three straight lines. The working conditions for the experiment and analysis are shown in Table 1. The lubricant for nosing was metal working oil G-3244, which was developed by Nihon Kohsakuyu Co., Ltd. for forming aluminum alloy.

In the experiment, the tube was pushed until one of the defects occurred. Buckling was defined as increase of diameter of the tube by more than 2 % from the original tube. Polygonal wrinkle, split and wrinkle were examined by visual reference. The diameter of the tube tip was measured at every 1 mm increase of pushing stroke, and the presence and mode of the defect were recorded. The forming limit was evaluated by limit nosing ratio κ_L which was defined by the following equation.

$$\kappa_L = \frac{D_0 - D_L}{D_0} \quad (1),$$

where, D_0 is initial diameter of the tube tip and D_L is limit diameter, which is the minimum diameter of a tube tip without any defects.

A model for numerical analysis is shown in Fig. 5 and the conditions for finite element analysis (FEA) are shown in Table 2. Elastic-plastic analysis was carried out for estimation of the deformation of the tube tip and pushing force during processing, which was not able to be measured in the experiment. In analysis, the commercial code ELFEN, which was developed by Rockfield Software Limited, Swansea, was used. A 3D dynamic explicit scheme was applied and a von Mises' yield criterion was adopted. The element type of the tube was a solid hexahedron and that of the die was a shell. The die was rotated and pressed over the tube tip while the other end of the tube was constrained. The heat generation by plastic deformation and friction would be smaller than heat dissipation, so the temperature change was neglected in analysis, as the tube temperature was low (about 20 °C) in the experiment. The friction coefficient was assumed to be 0.25 so that the forming limit might be equal to the experimental results in simple press forming. The usage of FEA does not focus on the quantitative prediction of defect occurrence, but on the qualitative examination of the deformation mechanism which leads to defects. The analysis was conducted based on a validity check on the defect occurrence in axisymmetric nosing, which was conducted by the authors, Kuboki et al. (2008).

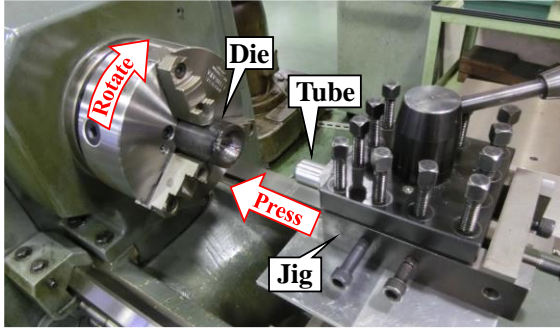


Fig. 3. Photograph of experimental set-up.

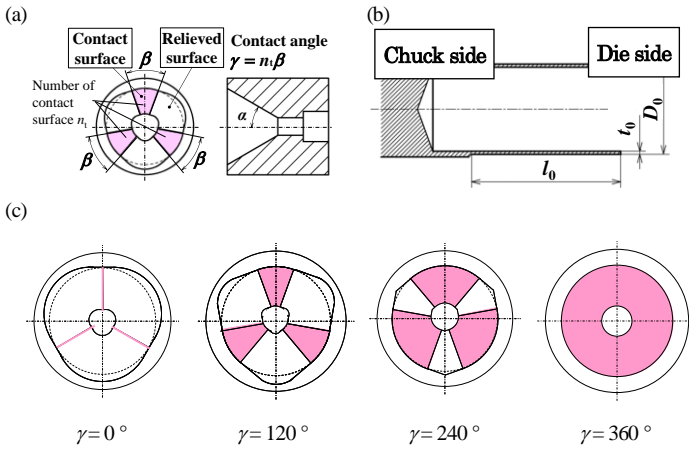


Fig. 4. Outline of relieved die and tube. (a) Relieved die, (b) Tube, (c) Schematics for various contact angles.

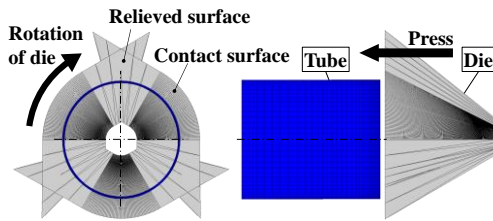


Fig. 5. FEM model.

3.2. Experimental and numerical results

Table 3 shows nosed tubes with defects, which were formed just beyond the forming limit in one-step nosing. The limit nosing ratio κ_L and defect modes in the experiment are shown in Fig. 6. Split occurred after occurrence of polygonal wrinkle with die of contact angle γ of 60° . It was revealed that split or polygonal wrinkle occurred with a die of small contact angle γ and buckling occurred with a die of a larger angle as shown in Fig. 6. In addition, wrinkle occasionally occurred with the die of contact angle γ of 360° , which resulted in excessive material due to no relief area. When a wrinkle occurred, the limit nosing ratio κ_L was 0.16 denoted by (A).

Table 1. Experimental and analysis conditions.

Working condition	Feed of tube f / mm-rev ⁻¹	0.1
	Number of revolutions N / rpm	140
	Lubrication	Oil
Die	Half angle α / °	30
	Number of contact surfaces n_t	3
	Contact angle γ / °	0, 60, 120, 180, 240, 300, 360
	Material	SKD11
Tube	Diameter D_0 / mm	30
	Length l_0 / mm	35
	Thickness t_0 / mm	0.5
	Thickness ratio t_0/D_0 (%)	1.7
	Material	A6063





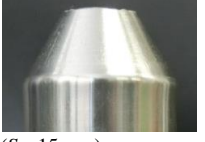
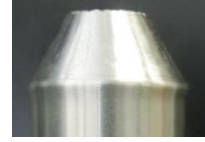


Table 2. Conditions for finite element analysis.

Software	ELFEN	
Friction coefficient μ	0.25	
Number of elements of tube	Thickness N_t	4
	Longitude N_l	32
	Hoop N_h	64
Analysis scheme	3D dynamic explicit	

Fig. 7 shows the radius history of one node at the tube tip during one rotation at pushing stroke S of 1.5 mm in analysis. When contact angle γ was small, the diameter of the tube tip was not sufficiently reduced and the tube tip largely stretched out. Since the stretch-out cyclically occurred, split occurred by accumulation of damage. When the damage was not accumulated to a certain amount, polygonal wrinkle appeared. Thus, split or polygonal wrinkle occurs with a die of smaller contact angle. The history of pushing force P was obtained by the analysis as shown in Fig. 8. Pushing force P increased with the increase of pushing stroke S and contact angle γ . Buckling occurred for larger contact angles as the pushing force P increased.

The history of thickness of a tube tip was obtained by the analysis as shown in Fig. 9. Generally, split tends to occur with decrease of the thickness t . However, there was no correlation between defect occurrence and thickness t . Fig. 10 shows the history of hoop stress of one node at the tube tip during one rotation at pushing stroke S of 1.5 mm in analysis. When contact angle γ was small, the hoop stress σ_θ increased in the tensile direction. The large tensile hoop stress decreases shrinkage of the tube tip during one rotation of the die. Thus, the tube tip largely stretched out and split or polygonal wrinkle occurred. When contact angle γ was large, the hoop stress σ_θ increased in the compression direction. The large compressive hoop stress caused increase of pushing force and buckling.

Table 3 Nosed tubes with defects, which were formed just beyond the forming limit in one-step nosing.

Contact angle / °	0	60	120	180
Nosed tube (Pushing stroke)	 ($S = 4$ mm)	 ($S = 4$ mm)	 ($S = 4$ mm)	 ($S = 11$ mm)
Defect mode	Polygonal wrinkle	Polygonal wrinkle	Polygonal wrinkle	Split
Contact angle / °	240	300	360 (A)	360 (B)
Nosed tube (Pushing stroke)	 ($S = 15$ mm)	 ($S = 15$ mm)	 ($S = 4$ mm)	 ($S = 11$ mm)
Defect mode	Buckling	Buckling	Wrinkle	Buckling

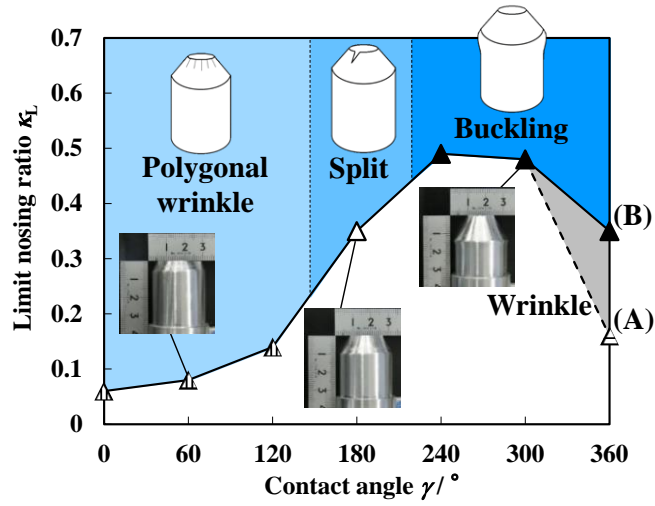


Fig. 6. Limit nosing ratio κ_L and defect mode of one-step nosing (Experiment).

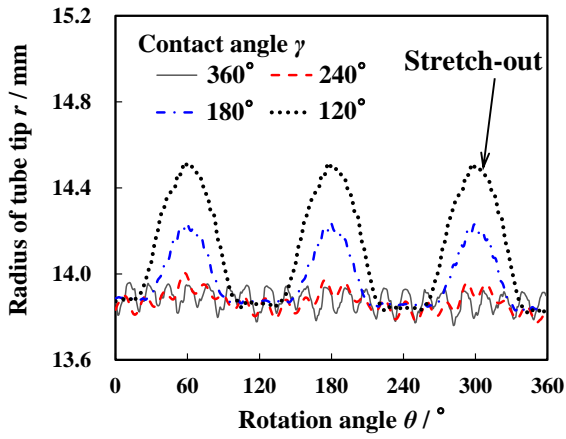


Fig. 7. Radius of tube tip (FEM).

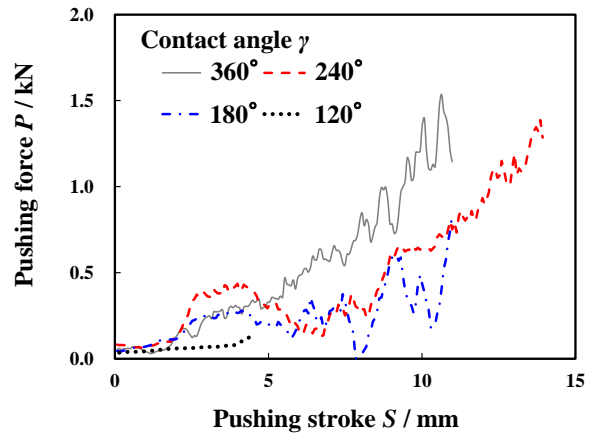


Fig. 8. Pushing force (FEM).

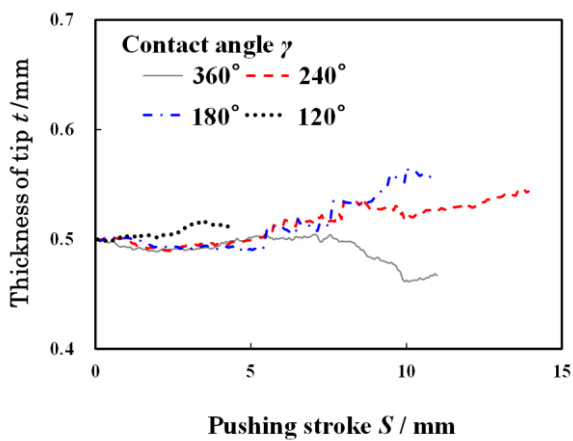


Fig. 9. Thickness of tube tip (FEM).

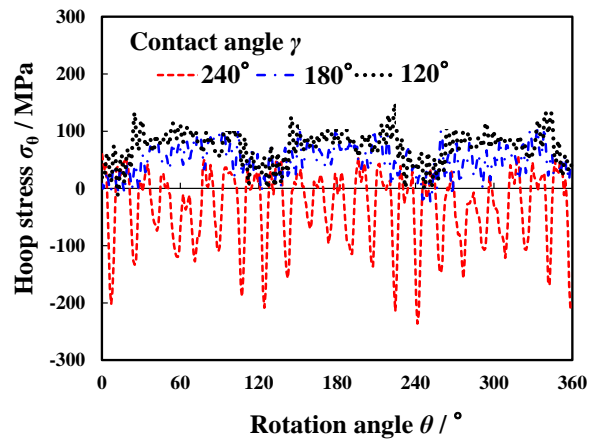


Fig. 10. Hoop stress (FEM, initial yield stress $Y = 123$ MPa).

4. Two-step nosing

4.1. Forming conditions

Fig. 11 (a) shows schematic illustration of two-step nosing and Fig. 11 (b) shows the efficiency and superiority of two-step nosing in a conceptual manner. This study assumed the mechanism of defect occurrence as follows. Buckling occurs depending on the temporary value of the pushing force regardless of deformation history. On the other hand, polygonal wrinkle and split appear depending on accumulation of defect causes. In the case of polygonal wrinkle, the delay of shrinkage rate to the ideal rate accumulates, and the accumulated amount exceeds the threshold for wrinkle appearance. In the case of split, the damage accumulates inside the tube tip because of the cyclic stretch-out, and the accumulated amount exceeds the threshold. Therefore, two-step nosing would be effective for improvement of the limit nosing ratio. A die with large contact angle should be used at the 1st step for suppressing the accumulation of defect causes until the pushing force comes near the limit, and another die with smaller contact angle should be used at the 2nd step for suppression of the pushing force. The limit nosing ratio should be increased as the accumulation of defect causes would just start at the beginning of the 2nd stage if the accumulation is very small for the 1st step with the die of large contact angle.

Experimental and analysis conditions are shown in Table 4. The contact angles at first-step γ_1 were 240 and 300° and the contact angle at the second-step γ_2 ranged from 0 to 180°, leading to the 8 combinations of dies in total. Nosing for the first-step was carried out until the pushing stroke S_1 reached 14 mm in both cases of the contact angle γ_1 of 240 or 300°, and nosing for the second-step was carried out in the cases of contact angle γ_2 of 0, 60, 120 and 180°.

A model for numerical analysis is shown in Fig. 12 and the conditions for finite element analysis are shown in Table 5. The model at the 2nd step employed the tube shape, which was generated from the geometrical information of the tools of the 1st step, neglecting work hardening by the 1st step. Two-step nosing was simulated by pressing the rotating die over the tube tip in a similar manner to the analysis of one-step nosing.

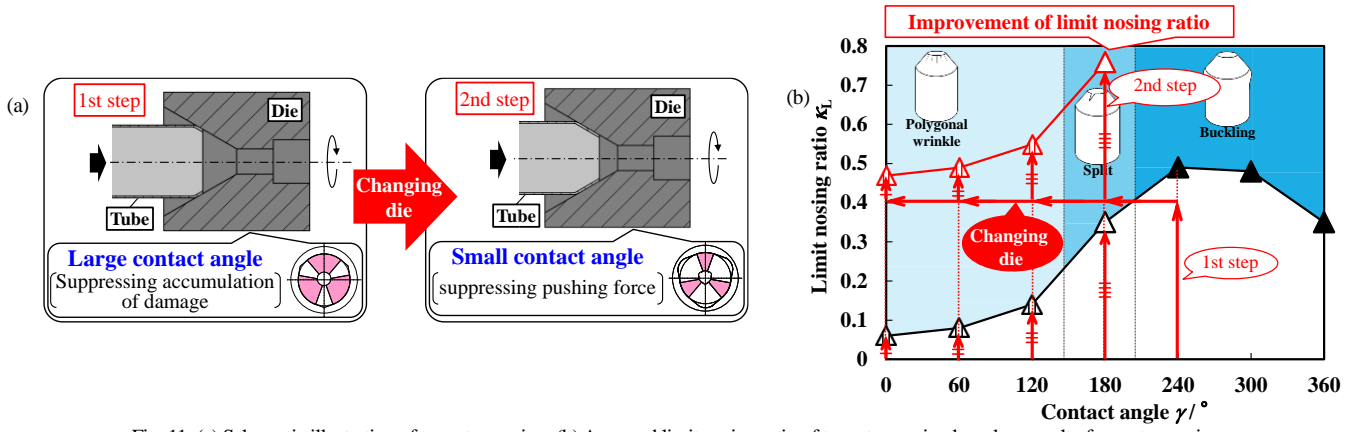


Fig. 11. (a) Schematic illustration of two-step nosing, (b) Assumed limit nosing ratio of two-step nosing based on result of one-step nosing.

Table 4 Experimental and analysis conditions.

Contact angle at first-step $\gamma_1 / ^\circ$	240, 300
Contact angle at second-step $\gamma_2 / ^\circ$	0, 60, 120, 180
Pushing stroke at first-step S_1 / mm	14

Table 5 Conditions for finite element analysis.

Tube tip diameter at the beginning of two-step nosing D_1 / mm	14.7
Tube length l_1 / mm	33.7

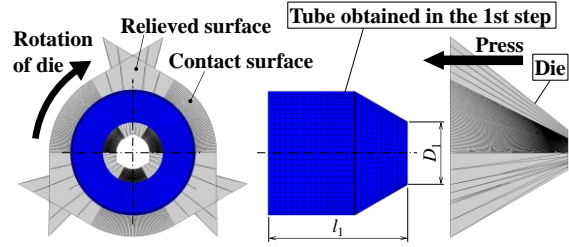


Fig. 12. FEM model for the 2nd step in two-step nosing.

4.2. Experimental and numerical results

Table 6 shows nosed tubes with defects, which were formed just beyond the forming limit in two-step nosing. Limit nosing ratio κ_L and the defect modes under each condition in the experiment are shown in Fig. 13. The result of one-step nosing is also shown in Fig. 13 for comparison. Imaginary lines C1 and C2 are shown in Fig. 13 as the limits for split, polygonal wrinkle and buckling of one-step nosing, which were assumed based on the result of the experiment in one-step nosing. Imaginary line C3 is also shown in Fig. 13, which was drawn by offsetting imaginary line C2 to the nosing ratio just before the buckling occurrence under the condition in which contact angle γ was 240° . The limit nosing ratio of two-step nosing is presumed to be placed on imaginary line C3 unless the nosing ratio reaches the limit for buckling, because the accumulation of damage is suppressed in the 1st-step by using a die with large contact angle. As shown in Fig. 13, limit nosing ratio clearly increased by application of the two-step method because the accumulation of defect, which causes split or polygonal wrinkle in the first step, was suppressed. Limit nosing ratio κ_L attained 0.58 under the optimum condition, in which the contact angle at the first-step γ_1 was 240° and the angle at the second-step γ_2 was 180° as denoted by [A]. The defect mode at [A] was buckling and [A] would be placed on the imaginary line C2, which would be extrapolated from the buckling limit

of one-step nosing. The history of pushing force P is shown in Fig. 14, which was obtained from the analysis. Pushing force P with a die of contact angle γ_2 of 180° was smaller than that of 240° as shown in Fig. 14. Thus, the forming limit was improved compared to one-step nosing with a die of contact angle γ of 240° due to suppression of buckling. Photographs of tubes at the highest forming limit of one-step and two-step nosing are shown in Fig. 15. It is clear from these photographs that the forming limit was improved by application of the two-step method.

Table 6 Pictures of nosed tubes which were formed by two-step nosing and defect mode which occurred under each condition.

Contact angle at the first-step $\gamma_1 / ^\circ$		Contact angle at the second-step $\gamma_2 / ^\circ$			
		0	60	120	180
240	Nosed tube (Pushing stroke)				
	Defect mode	Split	Split	Polygonal wrinkle	Buckling
300	Nosed tube (Pushing stroke)				
	Defect mode	Split	Split	Polygonal wrinkle	Buckling

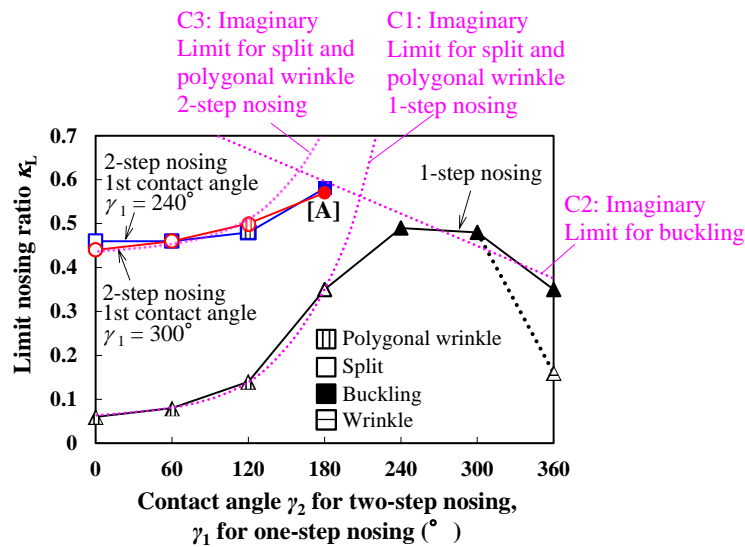


Fig. 13. Limit nosing ratio κ_L and defect mode of two-step nosing (Experiment).

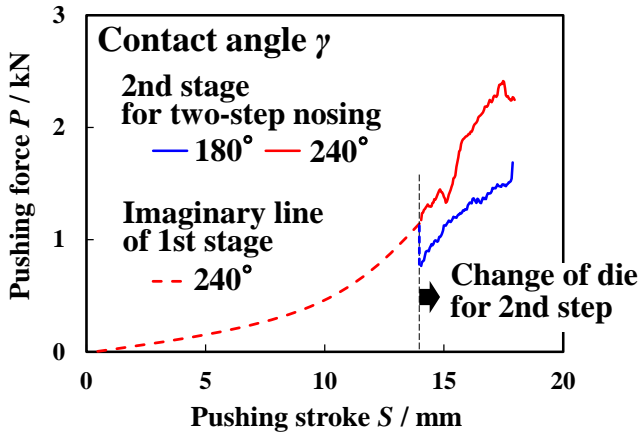


Fig. 14. Pushing force (FEM).

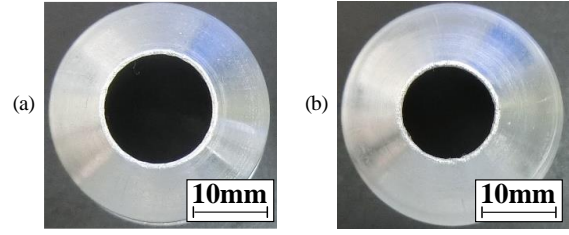


Fig. 15. Forming limit at the optimum condition.
 (a) One-step nosing ($\gamma = 240^\circ$, $\kappa_L = 0.49$),
 (b) Two-step nosing ($\gamma_1 = 240^\circ$, $\gamma_2 = 180^\circ$, $\kappa_L = 0.58$).

5. Eccentric nosing

5.1. Experimental conditions

An experiment was carried out for fabrication of eccentric tubes and its formability was investigated. In previous research, Kuboki et al. (2015) attained limit nosing ratio κ_L of 0.47 by one-step nosing using a relieved die for eccentricity δ_0 of 2 mm. In this research, two-step forming was applied to fabrication of eccentric tubes and its availability was examined in order to improve the forming limit. In addition, investigation of the optimum path line of the tube during the nosing process was carried out for further improvement of the forming limit. An experiment of "slant nosing" was conducted for a counter proposal to simple "straight nosing". "Slant nosing" may improve the forming limit by suppressing partial deformation which occurs due to partial contact between the tube tip and the die in "eccentric nosing". Fig. 16 shows the schematics of "straight nosing" for eccentric tube, where eccentricity δ_0 is set at the beginning of nosing and the tube is moved in a parallel way to the die axis. Fig. 17 shows the schematic of "slant nosing". In slant nosing, the tube is coaxially arranged to the die at the beginning of nosing, and eccentric tube is formed by applying constant displacement to a tube in a direction perpendicular to the central axis of the die. Application of slant nosing may suppress partial deformation which is caused by partial contact of the tube tip to the die and be able to improve the forming limit.

The experimental conditions for eccentric nosing are shown in Table 7. The contact angle at the first-step γ_1 was 240° and the contact angle at the second-step γ_2 was 180° , which realized the highest limit nosing ratio κ_L in

axisymmetric two-step nosing. Eccentricity $\Delta\delta_0$ was 0, 2, 4 and 6 mm. One-step nosing was also carried out under the condition in which the contact angle γ was 240° for comparison. The experimental conditions for slant nosing are shown in Table 8. In the experiment of slant nosing, the effect on the feed for eccentricity per 1-mm axial feed $\Delta\delta_0$ on limit nosing ratio κ_L was investigated. Straight nosing was also carried out. Straight nosing is simple eccentric nosing in which a tube is pressed parallel to the central axis of the die. The effect of application of slant nosing was verified by comparing them.

One-step nosing	Contact angle $\gamma / ^\circ$	240
Two-step nosing	Contact angle at first-step $\gamma_1 / ^\circ$	240
	Contact angle at second-step $\gamma_2 / ^\circ$	180
Amount of eccentricity δ_0 / mm		0, 2, 4, 6

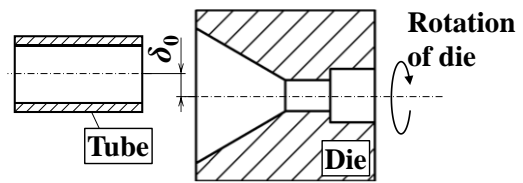


Fig. 16. Schematic of straight nosing for eccentric tube.

Contact angle $\gamma / ^\circ$	240, 180
Feed for eccentricity per 1-mm axial feed $\Delta\delta_0 / \text{mm}$	0.4, 0.6

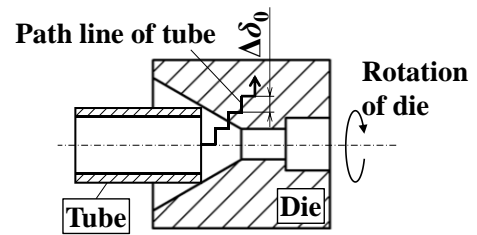


Fig. 17. Schematic of slant nosing for eccentric tube.



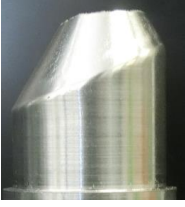

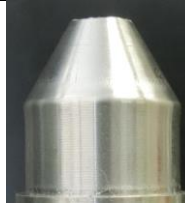
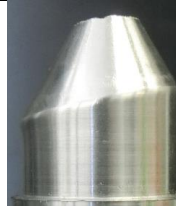


5.2 Experimental results

Photos of nosed tubes which were formed by one-step and two-step eccentric nosing and defect modes are shown in Table 9. As a result of the experiment, the limit diameter of tube tip D_L was not able to be measured in some tubes as defects occurred before all of the tube tip contacted the inner surface of the die in straight nosing as shown in Fig. 18. Therefore, the forming limit was evaluated by measuring limit pushing stroke S_L , which is the maximum pushing stroke without any defects. Limit pushing stroke S_L and the defect mode under each condition in the experiment are shown in Fig. 19. Limit pushing stroke S_L was improved by application of two-step forming under the condition of eccentricity δ_0 of 0 and 2 mm. However, the forming limit was not improved under the condition of eccentricity δ_0 of 4 and 6 mm. Generatrix lines between the die and tube at the forming limit are shown in Fig. 20. The length of the generatrix line with eccentricity δ_0 of 4 mm is larger than that of 0 mm as shown in Fig. 20.

As length of the contact line is increased, stretch-out in the relief area becomes larger and split tends to occur. As a result, the defect mode changed from buckling to split by application of two-step nosing in which the die was changed to one with a small contact angle at the 2nd stage in the process. Thus, two-step nosing was effective for forming eccentric tubes, however, the effect was decreased in case of large eccentricity.

Pictures of nosed tubes which were formed by slant and straight nosing and defect modes are shown in Table 10, and the limit nosing ratios κ_L of slant and straight nosing are shown in Table 11. The forming limit was not improved by application of slant nosing under the condition in which $\Delta\delta_0$ was 0.4 mm and γ was 240°. The improvement of slant nosing was also not obtained under the condition in which $\Delta\delta_0$ was 0.6 mm and γ was 180°. Under the condition in which $\Delta\delta_0$ was 0.6 mm and γ was 240°, defect occurred before all of the tube tip contacted the inner surface of the die in straight nosing, however, κ_L of 0.26 was obtained in slant nosing. In slant nosing, partial deformation was suppressed because all of the tube tip contacted the inner surface of the die from the beginning to the end of the nosing process. Therefore, slant nosing is safer than straight nosing as the tip shape of the nosed tube is always circular.

Table 9 Pictures of nosed tubes which were formed by one-step and two-step eccentric nosing and defect modes.

Contact angle / °		Eccentricity δ_0 / mm			
		0	2	4	6
240 (One-step)	Nosed tube				
	Defect mode	Buckling	Buckling	Buckling	Buckling
240 → 180 (Two-step)	Nosed tube				
	Defect mode	Buckling	Buckling	Split	Split

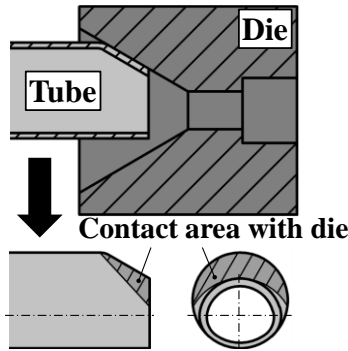


Fig. 18. Outline of tube before all of tube tip contacted inner surface of die.

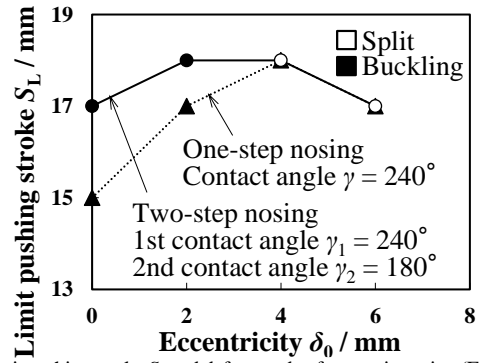


Fig. 19. Limit pushing stroke S_L and defect mode of eccentric nosing (Experiment).

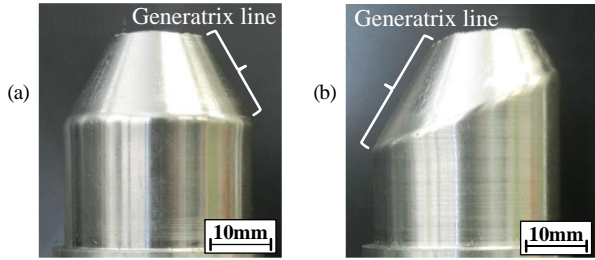


Fig. 20. Generatrix line between die and tube at forming limit (One-step nosing, contact angle $\gamma = 240^\circ$).

- (a) Eccentricity $\delta_0 = 0$ mm, pushing stroke $S = 15$ mm,
- (b) Eccentricity $\delta_0 = 4$ mm, pushing stroke $S = 18$ mm.

Table 10 Pictures of nosed tubes which were formed by slant and straight nosing and defect modes.

Contact angle $\gamma / ^\circ$		Feed for eccentricity per 1-mm axial feed $\Delta\delta_0 / \text{mm}$			
		0.4		0.6	
		Slant	Straight	Slant	Straight
180	Nosed tube	--	--		
	Defect mode	--	--	Split	Split
240	Nosed tube				
	Defect mode	Buckling	Buckling	Buckling	Buckling

-- : Not implemented

Table 11 Limit nosing ratio κ_L of slant and straight nosing.

Contact angle $\gamma / ^\circ$	Feed for eccentricity per 1-mm axial feed $\Delta\delta_0 / \text{mm}$			
	0.4		0.6	
	Slant	Straight	Slant	Straight
180	--	--	0.22	0.22
240	0.42	0.42	0.26	**

-- : Not implemented

** : Defect occurred before all of the tube tip contacted the inner surface of die.

6. Conclusion

As a result of a series of experiments and numerical analyses of one-step nosing, the mechanism of the occurrence of defects in rotary nosing with a relieved die was revealed. Split or polygonal wrinkle occurred when the contact angle was small, and FEA results showed it would be attributed to cyclic stretch-out occurring in the relief area of a die. Buckling occurred when the contact angle was large, and the FEA results showed it would be attributed to the increase of pushing force. Split or polygonal wrinkle occurred in contact angle γ of 0 - 180° and buckling occurred in contact angle γ of 240 - 360° in this research. In addition, improvement of limit nosing ratio κ_L was realized by application of two-step nosing in which a die with large contact angle was used at the 1st stage and the die changed to one with small contact angle just before buckling occurred at the 1st stage. Limit nosing ratio κ_L of 0.58 was obtained under the optimum condition of contact angle at first-step γ_1 of 240° and contact angle at second-step γ_2 of 180°. The result was much larger than limit nosing ratio κ_L of 0.49 by one-step nosing under the optimum condition. The forming limit for forming eccentric tubes was improved by application of two-step nosing, however, the effect was not provided in the case of large eccentricity. Slant nosing for forming eccentric tubes was proposed. Experiments revealed that slant nosing is able to suppress partial deformation which is caused by partial contact of the tube tip to the die.

References

- Manabe, K., Nishimura, H., 1984. Contact pressure distributions in nosing and flaring of tubes with conical tool. J. Jpn. Inst. Light Met. 34 (8), 439-445 (in Japanese).
- Alves, M., Almeida, B., Rosa, P., Martins, P., 2006. End forming of thin-walled tubes. J. Mater. Process. Technol. 177 (1), 183-187.
- Kobayashi, K., Yoshimura, S., 2011. 565 Optimal Tool Path Generation for Nosing Process in Spinning of Magnesium Alloy Tubes Based on Fuzzy Model. J. Jpn. Soc. Mech. Eng. 60, 565 (in Japanese).

- Zoghi, H., Fullahi, A., Sayeafabi, M., 2012. Effect of feed and roller contact start point on strain and residual stress distribution in dome forming of steel tube by spinning at an elevated temperature. *Proc. Inst. Mech. Eng. Part B J. Eng. Manuf.* 226, 1880-1890.
- Becker, C., Tekkaya, A. E., Kleiner, M., 2014. Fundamentals of the incremental tube forming process. *CIRP Annals - Manufacturing Technology*, 63, 253-256.
- Kuboki, T., Ohde, Y., Murata, M., 2008. Improvement of forming limit by rotary nosing with relieved die. *Proc. Inst. Mech. Eng. Part B J. Eng. Manuf.* 222, 245-253.
- Kuboki, T., Kominami, A., Ohde, Y., Murata, M., 2008. Effect of temperature on tube extrusion and joining holed rib. *Steel Res. Int.* 79, 137-144.
- Katoh, K., Kondo, K., Ido, K., 1995. Redrawing Process during One Stroke for Increasing Cup Height. *Trans. Jpn. Soc. Mech. Eng. Ser. C.* 61 (582), 710-715 (in Japanese).
- Kuboki, T., Abe, M., Yamada, Y., Murata, M., 2015. Flexible rotary reduction of tube tips by dies with relief surfaces for attaining high forming limit and productivity. *CIRP Ann.* 65 (1), 269-272.

- Fig. 1. Rotary nosing with relieved die for reduction of tube tip.
- Fig. 2. Defect modes. (a) Split, (b) Polygonal wrinkle, (c) Buckling, (d) Wrinkle.
- Fig. 3. Photograph of experimental set-up.
- Fig. 4. Outline of relieved die and tube. (a) Relieved die, (b) Tube.
- Fig. 5. FEM model.
- Fig. 6. Limit nosing ratio κ_L and defect mode of one-step nosing (Experiment).
- Fig. 7. Radius of tube tip (FEM).
- Fig. 8. Pushing force (FEM).
- Fig. 9. Thickness of tube tip (FEM).
- Fig. 10. Hoop stress (FEM).
- Fig. 11. (a) Schematic illustration of two-step nosing, (b) Assumed limit nosing ratio of two-step nosing based on result of one-step nosing.
- Fig. 12. FEM model for the 2nd step in two-step nosing.
- Fig. 13. Limit nosing ratio κ_L and defect mode of two-step nosing (Experiment).
- Fig. 14. Pushing force (FEM).
- Fig. 15. Forming limit at the optimum condition. (a) One-step nosing ($\gamma = 240^\circ$, $\kappa_L = 0.49$), (b) Two-step nosing ($\gamma_1=240^\circ$, $\gamma_2=180^\circ$, $\kappa_L=0.58$).
- Fig. 16. Schematic of straight nosing for eccentric nosing.
- Fig. 17. Schematic of slant nosing for eccentric nosing.
- Fig. 18. Outline of tube before all of the tube tip contacted the inner surface of the die.
- Fig. 19. Limit pushing stroke S_L and defect mode of eccentric nosing (Experiment).
- Fig. 20. Generatrix line between die and tube at forming limit (One-step nosing, contact angle $\gamma = 240^\circ$).
 (a) Eccentricity $\delta_0 = 0$ mm, pushing stroke $S = 15$ mm, (b) Eccentricity $\delta_0 = 4$ mm, pushing stroke $S = 18$ mm.

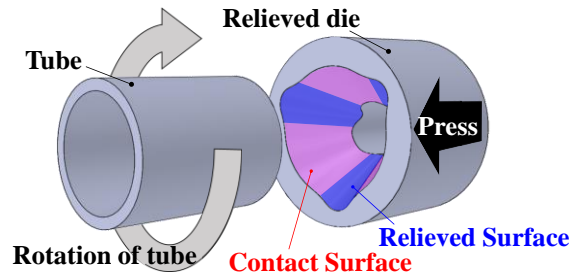


Fig. 1. Rotary nosing with relieved die for reduction of tube tip.

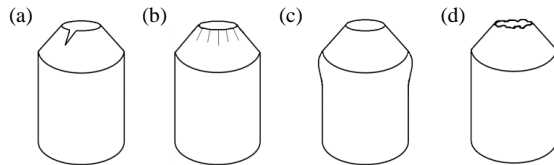


Fig. 2. Defect modes. (a) Split, (b) Polygonal wrinkle, (c) Buckling, (d) Wrinkle.

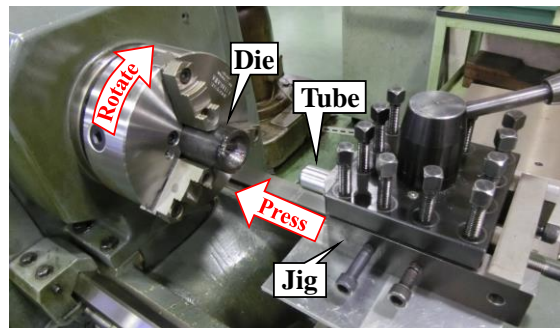


Fig. 3. Photograph of experimental set-up.

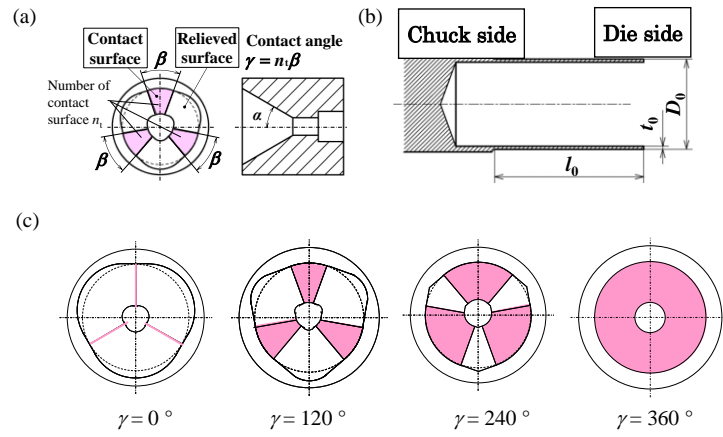


Fig. 4. Outline of relieved die and tube. (a) Relieved die, (b) Tube, (c) Schematics for various contact angles.

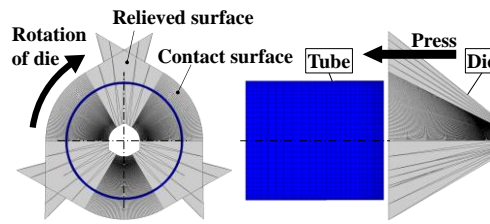


Fig. 5. FEM model.

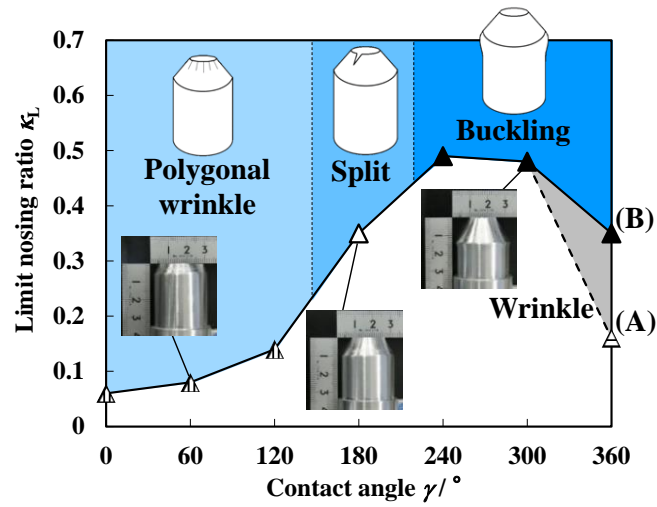


Fig. 6. Limit nosing ratio κ_L and defect mode of one-step nosing (Experiment).

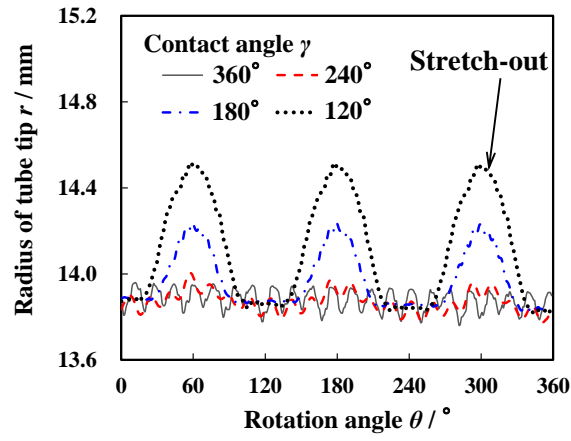


Fig. 7. Radius of tube tip (FEM).

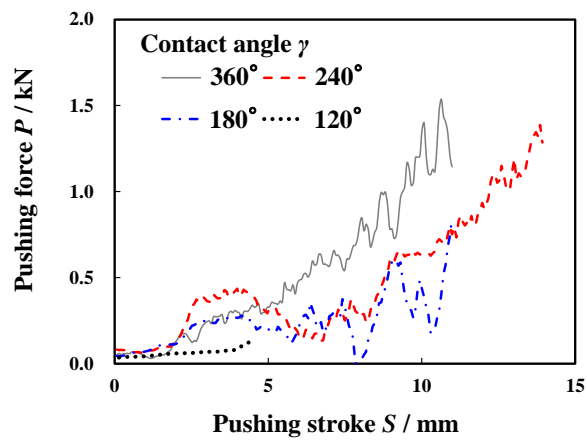


Fig. 8. Pushing force (FEM).

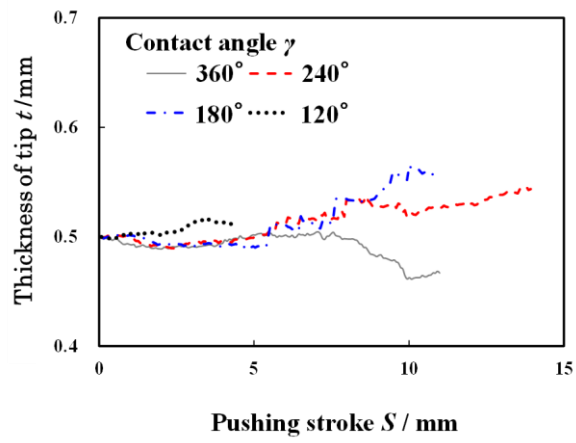


Fig. 9. Thickness of tube tip (FEM).

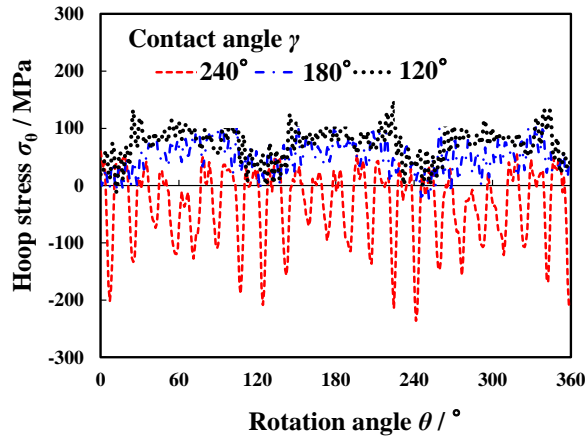


Fig. 10. Hoop stress (FEM, initial yield stress $Y=123$ MPa).

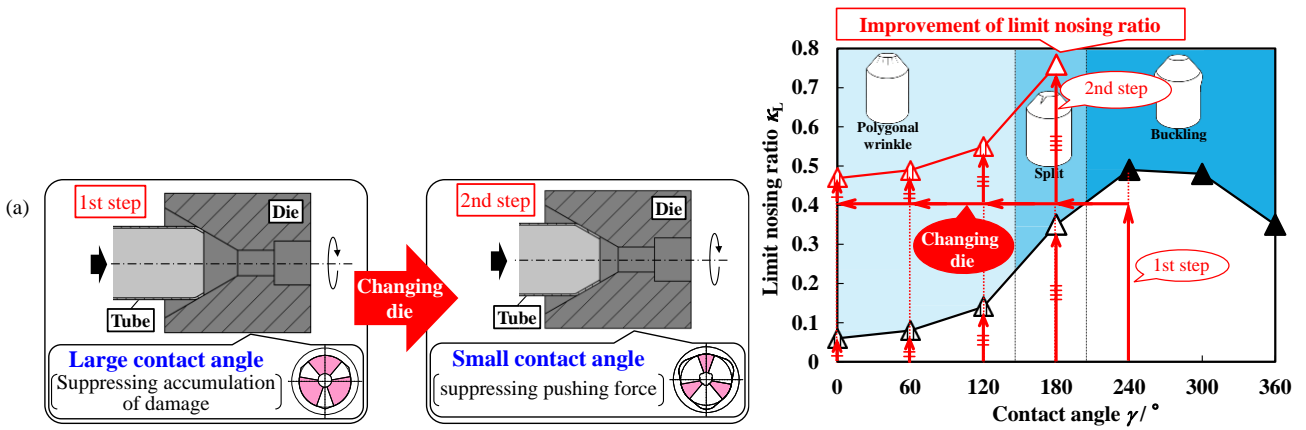


Fig. 11. (a) Schematic illustration of two-step nosing. (b) Assumed limit nosing ratio of two-step nosing based on result of one-step nosing.

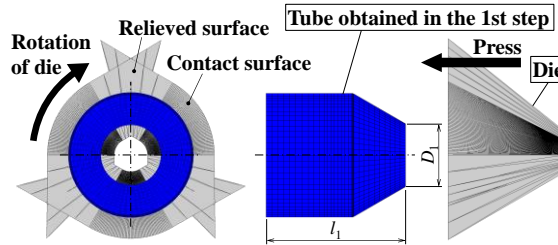


Fig. 12. FEM model for the 2nd step in two-step nosing.

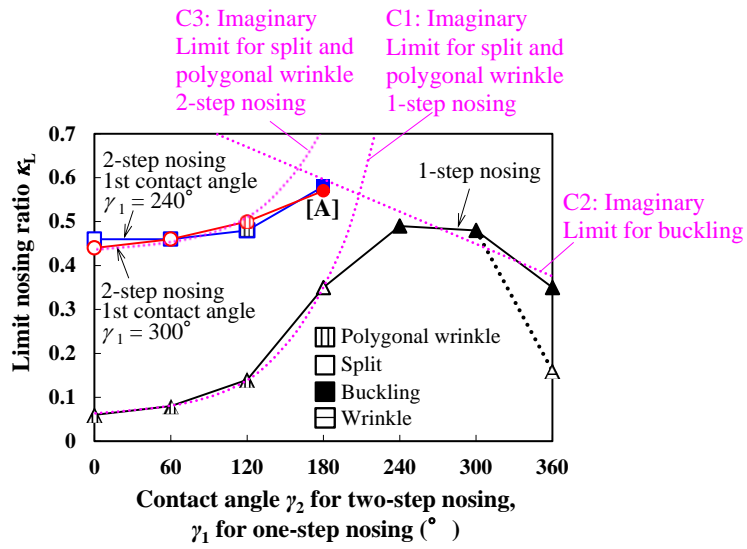


Fig. 13. Limit nosing ratio κ_L and defect mode of two-step nosing (Experiment).

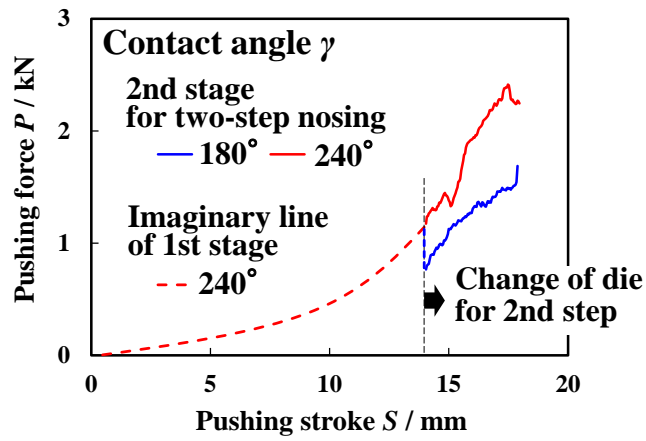


Fig. 14. Pushing force (FEM).

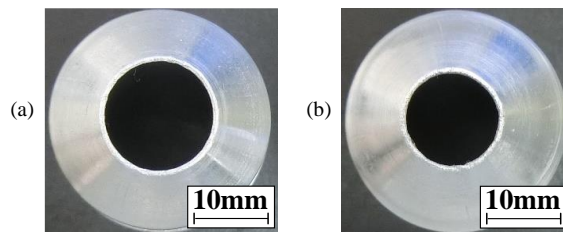


Fig. 15. Forming limit at the optimum condition. (a) One-step nosing ($\gamma = 240^\circ$, $\kappa_L = 0.49$), (b) Two-step nosing ($\gamma_1=240^\circ$, $\gamma_2=180^\circ$, $\kappa_L=0.58$).

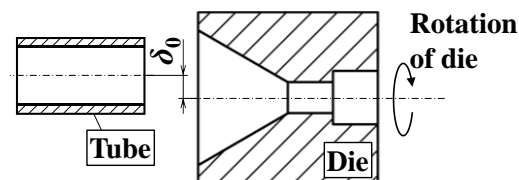


Fig. 16. Schematic of straight nosing for eccentric nosing.

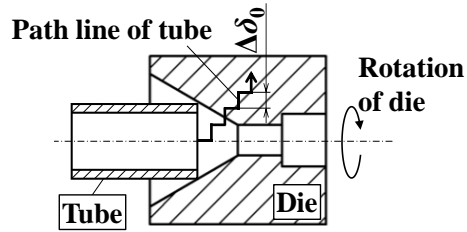


Fig. 17. Schematic of slant nosing for eccentric nosing.

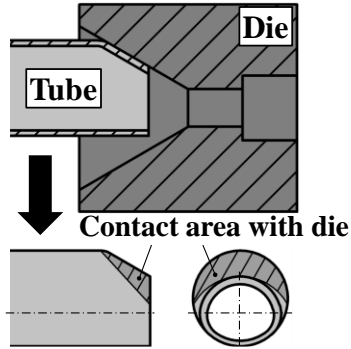


Fig. 18. Outline of tube before all of the tube tip contacted the inner surface of the die.

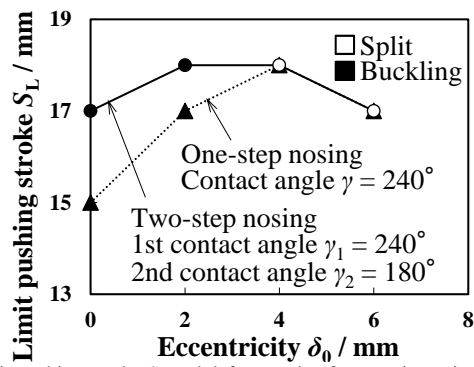


Fig. 19. Limit pushing stroke S_L and defect mode of eccentric nosing (Experiment).

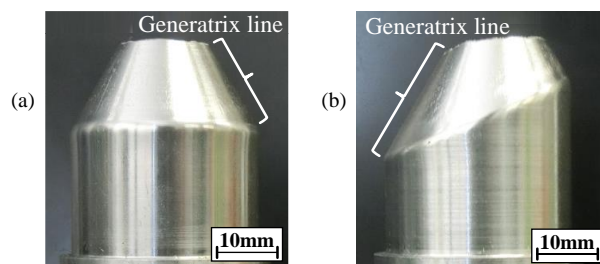


Fig. 20. Generatrix line between die and tube at forming limit (One-step nosing, contact angle $\gamma = 240^\circ$).
 (a) Eccentricity $\delta_0 = 0$ mm, pushing stroke $S = 15$ mm, (b) Eccentricity $\delta_0 = 4$ mm, pushing stroke $S = 18$ mm.

Table 1. Experimental and analysis conditions.

Table 2. Conditions for finite element analysis.

Table 3 Nosed tubes with defects, which were formed just beyond the forming limit in one-step nosing.

Table 4 Experimental and analysis conditions.

Table 5 Conditions for finite element analysis.

Table 6 Pictures of nosed tubes which were formed by two-step nosing and defect mode which occurred under the each condition.

Table 7 Working conditions for eccentric nosing.

Table 8 Working conditions for slant nosing.

Table 9 Pictures of nosed tubes which were formed by one-step and two-step eccentric nosing and defect modes.

Table 10 Pictures of nosed tubes which was formed by slant and straight nosing and defect modes.

Table 11 Limit nosing ratio κL of slant and straight nosing.

Table 1. Experimental and analysis conditions.

Working condition	Feed of tube $f / \text{mm} \cdot \text{rev}^{-1}$	0.1
	Number of revolutions N / rpm	140
	Lubrication	Oil
Die	Half angle $\alpha / ^\circ$	30
	Number of contact surfaces n_t	3
	Contact angle $\gamma / ^\circ$	0, 60, 120, 180, 240, 300, 360
	Material	SKD11
Tube	Diameter D_0 / mm	30
	Length l_0 / mm	35
	Thickness t_0 / mm	0.5
	Thickness ratio t_0/D_0 (%)	1.7
	Material	A6063

Table 2. Conditions for finite element analysis.

Software	ELFEN	
Friction coefficient μ	0.25	
Number of elements of tube	Thickness N_t	4
	Longitude N_l	32
	Hoop N_h	64
Analysis scheme	3D dynamic explicit	

Table 3 Nosed tubes with defects, which were formed just beyond the forming limit in one-step nosing.




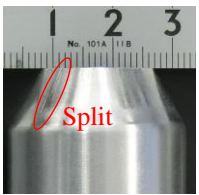
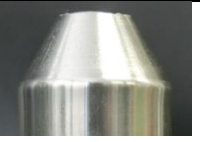
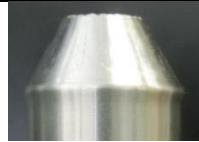

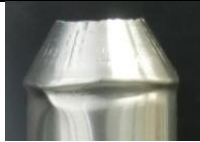
Contact angle / $^\circ$	0	60	120	180
Nosed tube (Pushing stroke)				
	($S = 4 \text{ mm}$)	($S = 4 \text{ mm}$)	($S = 4 \text{ mm}$)	($S = 11 \text{ mm}$)
Defect mode	Polygonal wrinkle	Polygonal wrinkle	Polygonal wrinkle	Split
Contact angle / $^\circ$	240	300	360 (A)	360 (B)
Nosed tube (Pushing stroke)				
	($S = 15 \text{ mm}$)	($S = 15 \text{ mm}$)	($S = 4 \text{ mm}$)	($S = 11 \text{ mm}$)
Defect mode	Buckling	Buckling	Wrinkle	Buckling

Table 4 Experimental and analysis conditions.

Contact angle at first-step $\gamma_1 / ^\circ$	240, 300
Contact angle at second-step $\gamma_2 / ^\circ$	0, 60, 120, 180
Pushing stroke at first-step S_1 / mm	14

Table 5 Conditions for finite element analysis.

Tube tip diameter at the beginning of two-step nosing D_1 / mm	14.7
Tube length l_1 / mm	33.7

Table 6 Pictures of nosed tubes which were formed by two-step nosing and defect mode which occurred under the each condition.

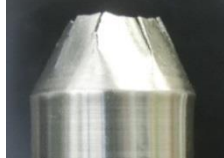
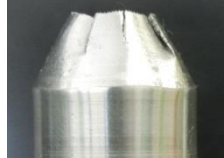
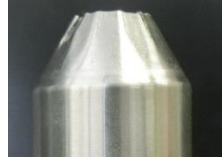
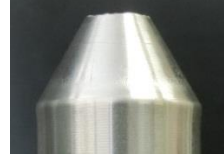


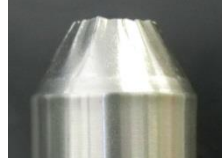

Contact angle at the first-step $\gamma_1 / ^\circ$		Contact angle at the second-step $\gamma_2 / ^\circ$			
		0	60	120	180
240	Nosed tube (Pushing stroke)				
	Defect mode	Split ($S = 14$ mm)	Split ($S = 14$ mm)	Polygonal wrinkle ($S = 15$ mm)	Buckling ($S = 17$ mm)
300	Nosed tube (Pushing stroke)				
	Defect mode	Split ($S = 14$ mm)	Split ($S = 14$ mm)	Polygonal wrinkle ($S = 15$ mm)	Buckling ($S = 17$ mm)

Table 7 Working conditions for eccentric nosing.

One-step nosing	Contact angle $\gamma / ^\circ$	240
Two-step nosing	Contact angle at first-step $\gamma_1 / ^\circ$	240
	Contact angle at second-step $\gamma_2 / ^\circ$	180
Amount of eccentricity δ_0 / mm		0, 2, 4, 6

Table 8 Working conditions for slant nosing.

Contact angle $\gamma / ^\circ$	240, 180
Feed for eccentricity per 1-mm axial feed $\Delta\delta_0$ / mm	0.4, 0.6

Table 9 Pictures of nosed tubes which were formed by one-step and two-step eccentric nosing and defect modes.


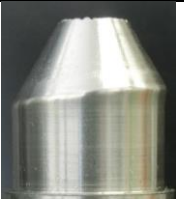
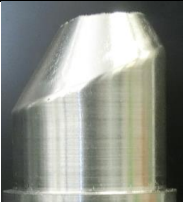
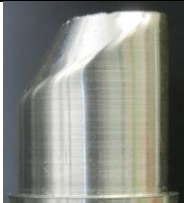
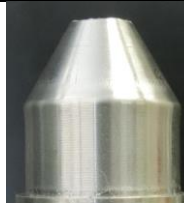
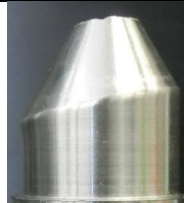
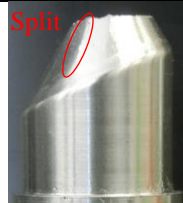







Contact angle / $^\circ$		Eccentricity δ_0 / mm			
		0	2	4	6
240 (One-step)	Nosed tube				
	Defect mode	Buckling	Buckling	Buckling	Buckling
240 → 180 (Two-step)	Nosed tube				
	Defect mode	Buckling	Buckling	Split	Split

Table 10 Pictures of nosed tubes which were formed by slant and straight nosing and defect modes.

Contact angle $\gamma / ^\circ$		Feed for eccentricity per 1-mm axial feed $\Delta\delta_0 / \text{mm}$			
		0.4		0.6	
		Slant	Straight	Slant	Straight
180	Nosed tube	--	--		
	Defect mode	--	--	Split	Split
240	Nosed tube				
	Defect mode	Buckling	Buckling	Buckling	Buckling

-- : Not implemented

Table 11 Limit nosing ratio κ_L of slant and straight nosing.

Contact angle $\gamma / ^\circ$	Feed for eccentricity per 1-mm axial feed $\Delta\delta_0 / \text{mm}$			
	0.4		0.6	
	Slant	Straight	Slant	Straight
180	--	--	0.22	0.22
240	0.42	0.42	0.26	**

-- : Not implemented

** : Defect occurred before all of the tube tip contacted the inner surface of the die.